Tuning Tailored Single-Walled Carbon Nanotubes by Highly Energetic Heavy Ions

El-Said, A. S.; Rao, S.; Akhmadaliev, S.; Facsko, S.;

Originally published:

April 2020

Physical Review Applied 13(2020)4, 044073

DOI: https://doi.org/10.1103/PhysRevApplied.13.044073

Tuning the Tailored Single-Walled Carbon Nanotubes by Highly Energetic Heavy Ions

Ayman S. El-Said[1],* Saleem Rao[1], Shavkat Akhmadaliev[2], and Stefan Facsko[2]
[1]*Physics Department, King Fahd University of Petroleum and Minerals, Dhahran 31261, Saudi Arabia and*
[2]*Institute of Ion Beam Physics and Materials Research,*
Helmholtz-Zentrum Dresden-Rossendorf (HZDR), 01328 Dresden, Germany

Carbon-based nanomaterials have attracted a lot of interest lately due to their highly promising applications. Here, we report on the modifications of single-walled carbon nanotubes (SWCNTs) induced by swift (highly energetic) heavy ions. Using scanning force microscopy and Raman spectroscopy, we observed a dramatic change in the structure of the irradiated SWCNTs, accompanied by an increase of the adhesion force as a function of ion fluence and electronic energy loss. With increasing ion fluence the SWCNTs exhibit a partial transformation from metallic to more semiconducting. Moreover, at high fluence they break into segments of 10–20 nm length.

PACS numbers: 79.20.Rf,34.35.+a,61.72.J-,61.80.Jh

Highly energetic heavy ions have become an important tool for modifying various materials for a wide range of applications in the last two decades[1,2]. This is mainly due to the high-energy deposition in a small volume along the ion track. Based on the material type and ion beam parameters, various swift-heavy ions (SHI) induced modifications are created not only in the structure but also in the mechanical, electronic and magnetic properties of the irradiated materials. Among the investigated samples, nanomaterials, such as carbon nanotubes (CNT) and in particular semiconducting single walled carbon nanotubes (SWCNTs), are the most promising one dimensional electronic materials with exceptional properties like high mobility in the range of 100.000 cm^2/Vs,[1–3] current densities of more than 10^9 A/cm^2, and on/off current ratios exceeding 10^5. These remarkable properties led to a wide range of applications in contemporary technologies such as CNT-based FET, biological sensors, drug delivery, energy storage, etc.[4–6]. In addition, SWCNTs have been explored as promising materials for electromagnetic interference (EMI) shielding, which is very important for electronic devices, such as laptops, cell phones, weather radars, TV picture transmitters etc. and in particular in space applications[7]. One might expect that ion irradiation should have the same effects on nanomaterials as on solid materials. However, it has recently been demonstrated that ion irradiation can induce novel and exciting effects on nanostructured materials. Examples are structural engineering of 2D materials, nanofabrication of quantum dots and self-assembly or self-organization in carbon nanosystems[8–10]. In fact, controlling the modifications induced in SWCNT is vital for tuning their mechanical, electrical and optical properties, as they strongly depend upon the chirality and present defects[11,12]. It was already demonstrated that the atomic structure and morphology of CNTs or related structures could be modified by ion irradiation[13,14]. They can even be interconnected or merged in a controllable way[15,16]. Despite the fact that ion irradiation of materials is usually introducing disorder/defects, recent experiments concerning ion irradiation of various nanostructures demonstrated that it could give provide unique effects[17–19]. Defect healing to useful localized modification has been reported under controlled heavy ion irradiation in carbon nanotubes[19–21]. Another important aspect is the presence of fast heavy ions in space environment, which makes studying their effects on the physical properties of SWCNTs essential for all possible space applications using SWCNTs. Here we present irradiation experiments of SWCNTs using highly energetic heavy ions in which the structure and the associated adhesion force is modified in a controlled way by simply tuning the ion fluence and the kinetic energy of the SHIs.

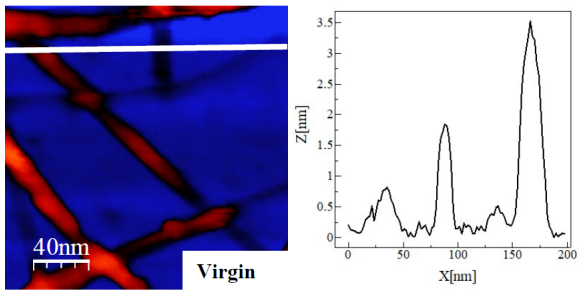

FIG. 1. Topographic SFM image and line profiles for SWCNTs on Si substrate.

Our experiments started with the sample preparation by immersing pre-cleaned commercially available silicon substrates in a solution of SWCNTs in dichlorobenzene (0.03 mg/mL) for 3 minutes. The CVD grown SWCNTs, of 1 nm in diameter were obtained from Sigma-Aldrich. After putting SWCNTs in dichlorobenzene, the mixture was sonicated for 10 min to get a homogenous suspension of SWCNTs in the solvent. The solution of SWCNTs was again sonicated for 1 min again just before dipping the silicon substrate. After removing the substrate from the SWCNTs-solution, it was dried under ambient condition without any rinsing. All samples were prepared from the same solution of SWCNTs following the same procedure. After preparation, the samples were irradiated at room temperature with swift iodine ions of various MeV kinetic energies and fluencies from the 6 MV Tandetron at HZDR (Dresden, Germany). The ion-

irradiated samples were inspected using Nanoscope III (Bruker) scanning force microscope (SFM). The microscope was operated in peak force tapping mode under ambient conditions using Bruker probe of 1.5 nN. This mode is based mainly on the acquisition of forcedistance curves at each pixel, which allows for the mapping of the elastic properties of the investigated surface. The image processing and analysis of SFM topographic images were performed using Nanotec Electronica SL WSxM software (version 5.0 Develop 6.4)[23]. In addition, Raman spectroscopy was performed to identify the induced defects in the irradiated SWCNTs.

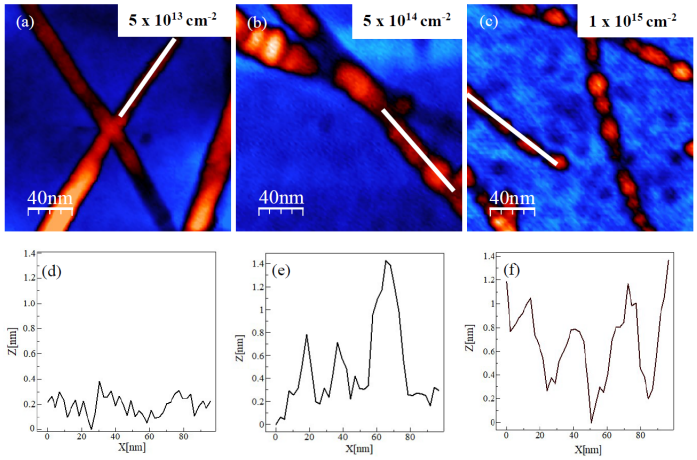

FIG. 2. Topographic SFM images (up) and line profiles for SWCNTs irradiated with 30 MeV iodine ions of various ion fluencies.

The energy deposition of SHIs in materials is proceeds via two channels: the electronic energy loss due to the interaction with the electronic system of the material and the nuclear energy loss transferring the ion energy to the target atoms via elastic collisions with the nuclei. For the high kinetic energies up to 54 MeV used in our experiments, the electronic energy loss dominates and consequently strong electronic excitations and ionisations along the ion track are induced. The utilized ion species and the corresponding parameters, as calculated by SRIM 2013[24], are listed in table I.

TABLE I. Parameters of the utilized iodine ions for irradiation of SWCNTs [kinetic energy (E_{kin}), ion fluence (φ), electronic stopping $(dE/dx)_e$, nuclear stopping $(dE/dx)_n$, mean range (R)] calculated using SRIM 2013.

Ions	E_{kin} (MeV)	$(dE/dx)_e$ (keV/nm)	$(dE/dx)_n$ (keV/nm)	R (μm)	φ (cm^{-2})
I^{+5}	20	6.03	0.30	5.11	5×10^{13}–10^{15}
I^{+6}	30	8.14	0.22	6.46	5×10^{12}–10^{15}
I^{+9}	54	11.4	0.14	8.84	5×10^{13}

The SFM topographic images in Fig. 1, 2, and 3 (a-c, i-k) are showing the virgin and irradiated samples with SWCNTs and their bundles of different sizes laying on the surface of Si substrates. Furthermore, the SFM images and the corresponding line profiles show clear deformation of the ion-irradiated tubes and their bundles into broken segments at high ion fluence. Moreover, the segments are getting smaller by increasing the ion fluence, as shown in Fig. 2. In addition to the measured topographic images, adhesion force mapping was performed simultaneously using the peak force-tapping mode giving the possibility to determine the adhesion force, between the tip and the tubes and the substrate. In this way, high-resolution images are acquired with detailed features, including the broken segments, of the ion-irradiated SWCNTs, as shown in Fig 3 (d-f, j-l). Figure 4 (a-g) shows the distributions of the adhesion force extracted from (1000 $\times$ 1000) nm^2 adhesion force images for SWCNTs irradiated with ion fluencies of 5×10^{13}–10^{15} and kinetic energies of 20 MeV, 30 MeV and 54 MeV, respectively. While the high peaks of histograms in Fig. 4 correspond to the substrates, the broad peak at smaller adhesion force represents the SWCNTs. The mean values of the adhesion forces were determined by fitting a gaussian function to each histogram for SWCNTs. The mean values of adhesion forces increase as a function of ion fluence from 2.2 ± 0.6 nN at $\varphi = 5\times10^{13}$ cm^{-2} to 4.0 ± 0.5 nN at $\varphi = 1\times10^{15}$ cm^{-2} of 30 MeV I ions. Only slight increase of the adhesion force as a function of electronic energy loss $(dE/dx)_e$ for the used iodine ions is observed, as shown in Fig. 4 (e, f, g). It is worthwhile mentioning that ion irradiation may lead to change of adhesion of the substrate. However, we paid attention only to the response of SWCNTs to ion irradiation.

The most prominent peaks in the measured Raman spectra are the disorder peak (D-peak), which is an indication of the presence of defects in SWCNTs, and the G-peak originating from longitudinal optical (LO) phonons. In SWCNTs, the G-band is spitted into two peaks, the G^-- and G^+-peaks (see Fig. 5), that originate from the LO modes in metallic and semiconducting nanotubes, respectively[25,26]. The high intensity and narrow profile of the G^+-peak in comparison to the broad G^--peak indicates that our virgin SWCNTs are more metallic. This reduction of the intensity and broadening of the G^--peak is mainly caused by the existence of the electron-phonon coupling in metallic nanotubes[26,27]. However, by increasing the ion fluence the Raman spectra show gradual change in the asymmetric G^--peak and the initially sharp G^+-peak, which can be ascribed to the partial transformation from metallic to semiconducting SWCNTs, as shown in Fig. 5. In addition, we observed more reduction in the intensity of G^--peak in comparison to G^+-peak for the ions exhibiting higher $(dE/dx)_e$. Furthermore, we observed that G^+-peak is getting relatively wider by increasing $(dE/dx)_e$ at the same ion fluence, see Fig. 6. This indicates that more defects are created in SWCNTS. This is demonstrated by observing an increase of the disorder parameter (I_D/I_G) as a function of ion fluence, as shown in Fig. 7. The I_D/I_G parameter in-

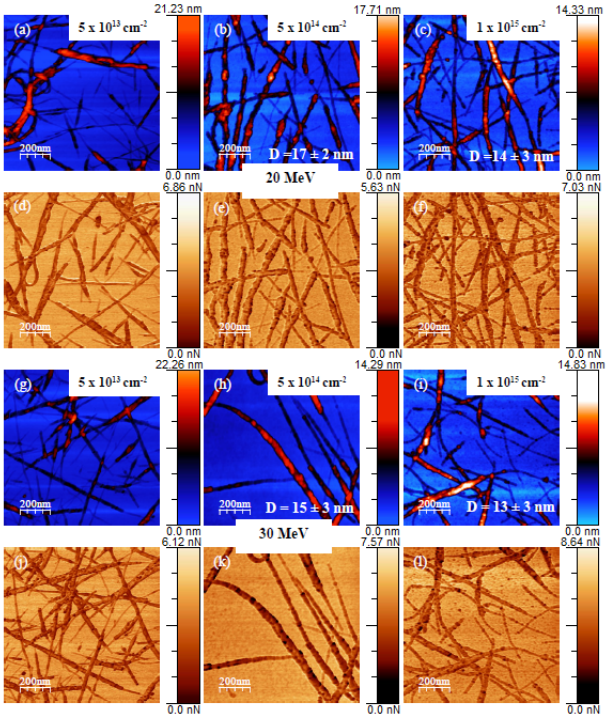

FIG. 3. Topographic SFM (a, b, c, g, h, i) adhesion force mapping (d, e, f, j, k, l) images of SWCNTs irradiated with 20 and 30 MeV iodine ions of various ion fluencies. The average size (D) of the broken segments is shown.

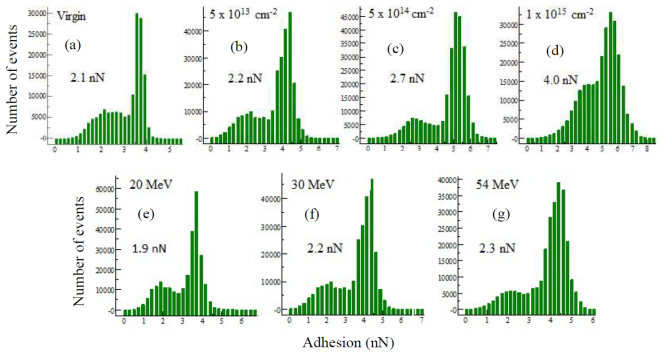

FIG. 4. Frequency distribution of adhesion force for virgin SWCNTs on Si substrates and irradiated with 30 MeV iodine ions of various ion fluencies (a, b, c, d). The histograms (e, f, g) are for SWCNTs irradiated with 5×10^{13} I ions/cm^2 of different kinetic energies. The mean value of adhesion force of SWCNTs is shown.

creases as a function of φ until it saturates at $\varphi = 5\times10^{13}$ cm^{-2} reaching a slightly smaller value at $\varphi = 1 \times 10^{15}$ cm^{-2}, which is an indication of defects healing, as already demonstrated in previous experiments using different ion species and kinetic energies[20,21]. Furthermore, it is also possible that ion induced amorphization occurs at high ion fluence[22]. This can be seen also form the deformation of the irradiated nanotubes.

Another extracted parameter from the measured Raman spectra is the crystallite size (L_d)[28], which is termed later inter-defects length (L_d), using TuinstraKoenig relation[29–32]. In opposite to I_D/I_G parameter, L_d is decreasing as a function of φ, which is ascribed to the creation of more defects by increasing ion fluence, as depicted in Fig. 7. Therefore, a higher disorder parameter and consequently smaller inter-defects length is observed at high fluence, where the SWCNTs are drastically damaged leading to breaking of the nanotubes into undamaged segments of length L_d. This agrees with the SFM observations of broken segments (D), which are getting smaller at higher ion fluence. Moreover, the size of the broken segments is estimated from the SFM images to be 10–20 nm, which is in fair agreement with the estimated L_d values, as shown in Fig. 2 and Fig. 7.

However, the fragmentation of the nanotubes is observed after surpassing from $\varphi = 5 \times 10^{13}$ cm^{-2}, which coincides with the fluence at which the saturation of the disorder parameter of SWCNTs occurs. The responsible defects for these effects are created by the coupling of the electron excitation induced by the MeV ions to

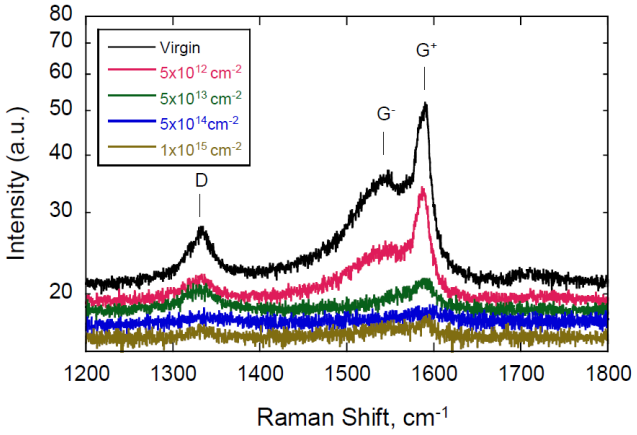

FIG. 5. Raman spectra of SWCNTs irradiated with 30 MeV I of different fluencies.

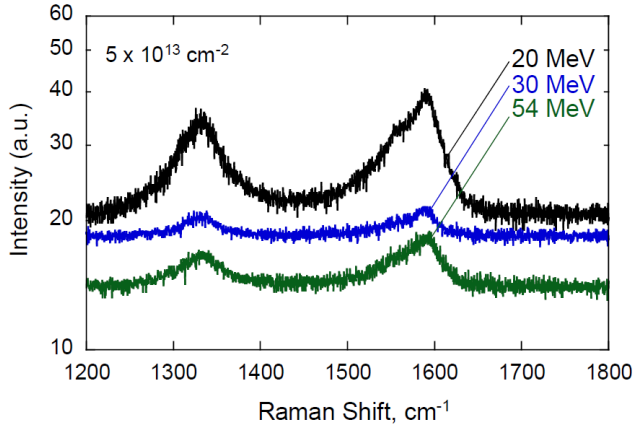

FIG. 6. Raman spectra of SWCNs irradiated with 5×10^{13} I ions/cm^2 of different kinetic energies.

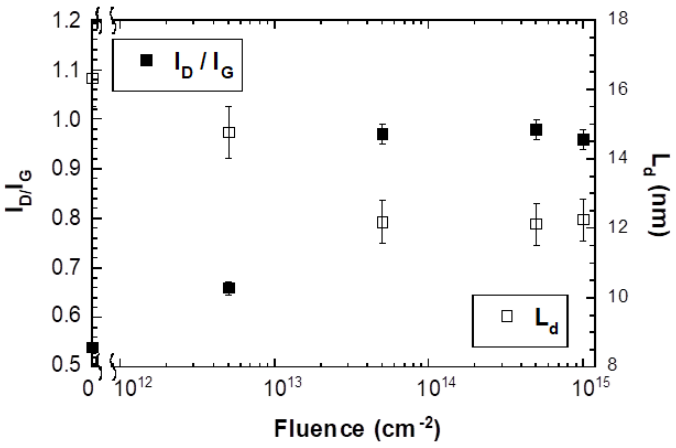

FIG. 7. Disorder parameter (I_D/I_G) and inter-defect length (L_d) as a function of ion fluence.

the phononic system. Within the concept of the thermal spike model, the electron-phonon coupling leads to a temperature increase in the irradiated zone, which causes structural modifications[33,34]. In addition, the observed modifications of SWCNTs are in agreement with the results of classical molecular dynamics simulations, which has shown that the irradiation with high ion fluence can lead to the breakup of nanotubes, amorphization, and partial/total loss of the tubular shape[22].

In conclusion, we have shown that swift heavy ions are able to modify single-walled carbon nanotubes in a controlled way. Ion-induced fragmentation of broken segments is observed as a function of ion fluence. The segments are observed only after surpassing an ion fluence threshold of 5×10^{13} cm^{-2}, which coincides with the fluence at which the disorder parameter measured with Raman spectroscopy saturates. In addition, we have demonstrated that the adhesion between the SFM probe and SWCNTs can be changed significantly by varying the ion fluence, and slightly by varying the electronic energy loss of the used ions.

ACKNOWLEDGEMENT

A. S. E. would like to acknowledge the support by KFUPM (Project No. ISSP1801). The assistance of A. Keller in peak force tapping measurements is appreciated. Parts of this research were carried out at the Ion Beam Center (IBC) of the Helmholtz-Zentrum Dresden-Rossendorf (HZDR), a member of the Helmholtz Association.

* *elsaid@kfupm.edu.sa*

[1] F. Aumayr, S. Facsko, A.S. El-Said, C. Trautmann and M. Schleberger, J. Phys.: Condens. Matter 23, 393001 (2011).
[2] A. Javey , G. Guo, Q. Wang, M. Lundstrom, H.J. Dai, Nature 424, 654 (2003).
[3] S. J. Tans, A. R. M. Verschueren, C. Dekker, Nature, 393, 49 (1998).
[4] F.L. Michael, D. Volder, S.H. Tawfick, R. H. Baughman, A.J. Hart, Science 339, 535 (2013).
[5] G. Wu, P. Tan, D. Wang, Z. Li, L. Peng, Y. Hu, C. Wang, W. Zhu, S. Chen, W. Chen, Sci. Reports 7, 43676 (2017).
[6] W. Kwak, K. Lau, C. Shin, K. Amine, L.A. Curtiss, Y. Sun, ACS Nano, 9 (4), 4129 (2015).
[7] L. Cai, C. Wang, Nanoscale Res. Lett 10, 320 (2015).
[8] A.V. Krasheninnikov, F. Banhart, Nat. Materials 6, 723 (2007).
[9] E Trynkiewicz, B R Jany, A Janas, F Krok, Phys. Condens. Matter 30, 304005 (2009).
[10] Z. Li and F. Chena, Appl. Phys. Rev. 4, 011103 (2017).
[11] Kim Y-H, Choi J, K. Chang, D. Tomnek, Phys. Rev. B 68 125420 (2003).
[12] M.Y.Han, B. zyilmaz, Y. Zhang, P. Kim, Phys. Rev. Lett. 98, 206805 (2007).
[13] D. Ugarte, Nature 359, 707 (1992).
[14] A. Kis, et al. Nature Mater. 3, 153(2004).
[15] M. Terrones, F. Terrones, Banhart, J.-C. Charlier, P. M. Ajayan, Science 288, 1226 (2000).
[16] M. Terrones, et al. Phys. Rev. Lett. 89, 075505 (2002).
[17] A.V. Krasheninnikov, K. Nordlund, J. Appl. Phys. 107, 071301 (2010).
[18] M.C. Ridgway, F. Djurabekova, K. Nordlund, Curr. Opin. Solid State Mater. Sci. 19, 29 (2015).
[19] D.K. Avasthi, Y.K. Mishra, F. Singh, J.P. Stoquert, Nucl. Instr. Meth. B 268, 3027 (2010).
[20] A. Kumar, D.K. Avasthi, J.C. Pivin, P.M. Koinkar, Appl. Phys. Lett. 92, 221904 (2008).
[21] A.V. Krasheninnikov, K. Nordlund, Nucl. Instr. Meth. B 216, 355 (2004).
[22] A.V. Krasheninnikov, K. Nordlund, J. Keinonen, F. Banhart, Phys. Rev. B 66, 245403 (2002).
[23] I. Horcas et al., Rev. Sci. Instr. 78, 013705 (2007).
[24] J.F. Ziegler, M.D. Ziegler, J. P. Biersack, Nucl. Instr. and Meth. B 268, 1818 (2010).
[25] K. Kempa, Phys. Rev. B 66, 195406 (2002).
[26] H. Telg. M. Fouquet, j. Maultzsch, Y. Wu, B. Chandra, J. Hone, T.F. Heinz, C. Thomsen, Phys. stat. sol. (b) 245, 2189 (2008).
[27] R. Krupke et al., Science 301, 344 (2003).
[28] F. Tuinstra, J.L. Koenig, J. Chem. Phys. 53, 1126 (1970).
[29] M.M. Lucchese, F. Stavale, E.H.M. Ferreira, C. Vilani, M.V.O. Moutinho, R.B. Capaz, C.A. Achete, A. Jorio, Carbon 48,1592 (2010).
[30] Vishalli, D.K. Avasthi, A. Srivastava, K. Dharamvir, Nucl. Instr. and Meth. B 407, 172 (2017).
[31] A. Olejniczak, V.A. Skuratov, Nucl. Instr. and Meth. B 326, 33 (2014).
[32] L.G Canado, A. Jorio, M.A. Pimenta, Phys. Rev. B 76, 064304 (2007).
[33] C. Dufour, V. Khomrenkov, Y.Y. Wang, F. Aumayr, M. Toulemonde, J. Phys: Condens. Matter 29, 095001 (2017).

[34] A.S. El-Said, R.A. Wilhelm, R. Heller, M. Sorokin, S. Facsko, F. Aumayr, Phys. Rev. Lett. 117, 126101 (2016).